Synthetic Aperture Radar Processing with Polar Formatted Subapertures

Armin W. Doerry

Sandia National Laboratories, Albuquerque, New Mexico

Abstract

Synthetic Aperture Radar (SAR) uses the motion of a small real antenna to synthesize a larger aperture, and thereby achieve very fine azimuth resolution. Efficient SAR image formation requires modelling the radar echo and compensating (focusing) the delay and phase for various positions in the target scene. Polar-Format processing is one successful algorithm developed to process large scenes at fine resolutions, but is still limited, especially at resolutions near a wavelength. This paper shows how using tiers of subapertures can overcome the limitations of Polar-Format processing and increase the focused scene size substantially while using only efficient vector multiplies and Fast Fourier Transforms.

1: Introduction and summary

The motion of a radar antenna relative to a target introduces a delay and phase in the echo that is a function of the antenna motion. When the antenna motion traces an arc, and the radar echoes are coherently collected, the signal data may be digitally processed to achieve an azimuth resolution much finer than that capable by the real antenna alone. In this way a virtual antenna array can be synthesized that may be many meters (or even kilometers) long. This technique is known as Synthetic Aperture Radar (SAR) processing, and is illustrated in figure 1. The distance function from each point on the aperture to each location in the scene being imaged is unique, that is, different for each location in the scene. Efficient processing of the data into a SAR image, however, necessitates using transform techniques which treat areas of the scene identically. The concept is to 'focus' to a scene center and use a transform such as the 2-dimensional Discrete Fourier Transform (DFT) to form an image of the area around the scene center. Locations not at the scene center will appear to move or 'migrate' around the scene center as the synthetic aperture is traced, thereby

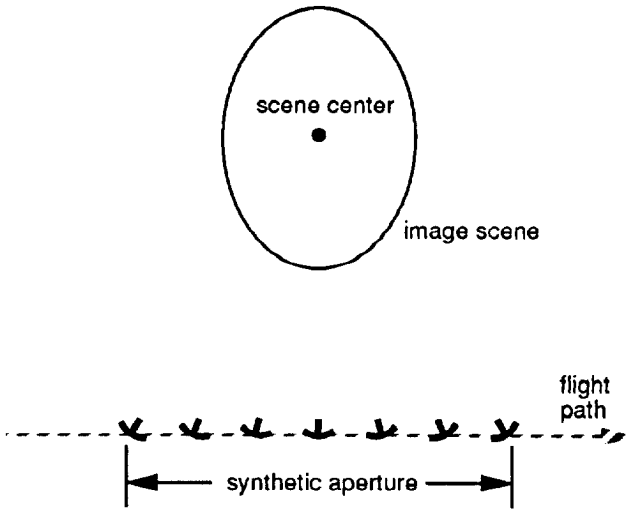

Figure 1: SAR Concept

smearing their response, and also suffer phase variations (defocusing) relative to the scene center. These effects worsen with distance from the scene center. After transformation into an image, the result is an image with worsening impulse response (broadening point spread function) as distance from the scene center increases. The degree of tolerance for image quality degradation at the scene edges limits the focused 'scene size'. The degradation, and hence scene size, is strongly affected by operating frequency and the resolution sought, with finer resolutions (longer synthetic apertures) and lower frequencies allowing smaller focused scene sizes [1]. The challenge for image formation algorithms is to focus a large scene at low frequencies and fine resolutions.

A number of image formation algorithms using various signal processing techniques have been proposed with various degrees of effectiveness in the low-frequency, fine resolution case. For airborne SAR, with its typically not-very-straight flight paths, a most effective technique is Polar-Format processing, first proposed by Walker [6]. But spatially variant phase errors limit the focused scene

1058-6393/95 $4.00

diameter D to

$$D \le 4\rho_x (\|r_{c0}\|/\lambda_0)^{1/2} \quad (1)$$

where ρ_x is the azimuth resolution, $\|r_{c0}\|$ is the nominal range, and λ_0 is the nominal radar wavelength.

One proposed solution is to divide an aperture into subapertures (sub-arrays) [2,5], and perhaps those subapertures into subsubapertures, and so on, in a tiered fashion to allow compensation of the phase errors that limit Polar-Format processing. Each subaperture would by itself be used to form a coarse resolution image using Polar-Format processing. The information extracted from the coarse resolution images is used to estimate appropriate phase corrections, whereupon processing occurs across co-located pixels in each of the coarse resolution images, again using Polar-Format processing, to form a finer resolution image, and so on. These stages form a pipeline architecture that uses only easily implemented vector multiplies and DFTs, to overcome the scene size barrier in equation (1). This paper shows how the new limit for scene size for this technique using N_s levels (tiers) of subapertures becomes

$$D \le 4\rho_x (\|r_{c0}\|/\lambda_0)^{\frac{(N_s+1)}{(N_s+2)}}. \quad (2)$$

2: One-dimensional analogy

Consider a function of the form

$$f(n) = \exp j\left(\omega n + a\omega^2 n^2\right), \quad (3)$$

with known constant a, $0 < a \ll 1$, unknown constant ω, $-\pi/2 \le -\Omega/2 \le \omega \le \Omega/2 < \pi/2$, and series index n, available over an aperture $N/2 \le n \le N/2 - 1$. The challenge is to determine ω with as fine a precision and accuracy as possible within the range $|\omega| \le \Omega/2$, and efficiently.

If a were zero, the task would simply amount to a Discrete Fourier Transform (DFT) across n and yield a resolution ρ in ω of about $2\pi/N$. For this case, larger N means finer resolution, without bound.

For nonzero a, we must consider the quadratic phase term (quadratic in n). For small Ω and small N, this term can be ignored. A reasonable criteria might be

$$a(\Omega/2)^2 (N/2)^2 \le \pi/2. \quad (4)$$

Performing an FFT across the data set limited by equation (4) then yields the constraint

$$\Omega \le \rho/\sqrt{\pi a/2}. \quad (5)$$

Here we see the basic dilemma. For using the DFT, or its efficient version, the Fast Fourier Transform (FFT), the larger Ω that we are interested in, the coarser the resolution is with which we can identify ω. The challenge becomes to exceed the limit in equation (5). To do this we need to mitigate the effects of the quadratic phase term which is an error term for FFT processing.

3: Subapertures

We do this by making a coarse resolution estimate of ω, and use this to compensate $f(n)$ before proceeding to a fine resolution estimate. Conceptually, we make coarse resolution estimates of ω by dividing the aperture into subapertures, as in figure 2(b). Mathematically, we do this by splitting the domain of index n into groups of indices m_1 and m_2, by making $n = m_1 + \Delta_2 m_2$, where m_1 is intra-subaperture index and is limited to the domain $-M_1/2 \le m_1 \le M_1/2 - 1$, m_2 is the inter-subaperture index and is limited to the domain $-M_2/2 \le m_2 \le M_2/2 - 1$, and Δ_2 is a data decimation factor, with subapertures overlapped by an amount $(M_1 - \Delta_2)$. Overlapping subapertures is necessary to control sidelobes. We rewrite the function $f(n)$ as

$$f(m_1, m_2) = \exp j\left(\omega(m_1 + \Delta_2 m_2) + a\omega^2 (m_1 + \Delta_2 m_2)^2\right). \quad (6)$$

The plan now is to perform a DFT across a much shorter ranged index m_1, and do this for each index value m_2, but first we need to examine the quadratic phase term $a\omega^2 m_1^2$. To keep this term's effects negligible, we choose M_1 such that

$$a(\Omega/2)^2 (M_1/2)^2 \le \pi/2. \quad (7)$$

With this restriction, a DFT of equation (6) yields approximately

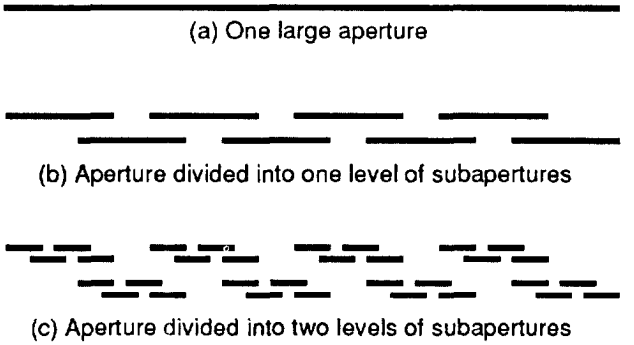

Figure 2. Aperture divided into subapertures, and subsubapertures

$$f_2(u_1, m_2) \approx$$

$$\text{csinc}_{M_1}\left[\frac{M_1}{2}\left(\omega + 2a\omega^2\Delta_2 m_2 - \frac{2\pi u_1}{M_1}\right)\right]$$

$$\times \exp j\left(\omega\Delta_2 m_2 + a\omega^2\Delta_2^2 m_2^2\right) \quad (8)$$

where we define $\text{csinc}_M(\,)$ as a convenient shorthand for the complex discrete sinc function, i.e.

$$\text{csinc}_M(x) \equiv \frac{\sin(x)}{\sin(x/M)} e^{-jx/M}. \quad (9)$$

The phase rotation in this function is typically negligible, especially in light of the amplitude envelope. In equation (8), the csinc function resolves ω with resolution $(2\pi/M_1)$, and locates it with the estimate

$$\hat{\omega} \approx 2\pi u_1/M_1 - 2a\hat{\omega}^2\Delta_2 m_2. \quad (10)$$

The problem here is that the estimate of ω depends on subaperture index value m_2, that is, the location of $\hat{\omega}$ 'migrates' with m_2. In fact, with large enough m_2, the migration will transcend several resolution cells (values of u_1). Therefor, for any one value of u_1, the migration has the effect of 'windowing' the data over index m_2, as the amplitude peak moves into and then out of the appropriate resolution cell u_1. Since we will ultimately want to perform a DFT across index m_2, it is desirable for the migration to be no more than about one coarse resolution cell ρ_1 in total, over all m_2 for any ω. This constrains

$$2a\left(\frac{\Omega}{2}\right)^2\Delta_2\left(\frac{M_2}{2}\right) \le \frac{1}{2}\left(\frac{2\pi}{M_1}\right), \quad (11)$$

which can be rewritten as,

$$\rho_1 = 2\pi/M_1 \ge a\Omega^2\Delta_2 M_2/2 \ . \quad (12)$$

Note that this is more severe than equation (7) since $\Delta_2 M_2 \gg M_1/2$. With this constraint, migration can be ignored in equations (8) and (10), and allows us to compensate, or 'focus', equation (8) prior to a DFT across m_2, by performing the phase adjustment

$$f_2^*(u_1, m_2) = f_2(u_1, m_2)$$

$$\times \exp j\left(-\hat{\omega}\Delta_2 m_2 - a\hat{\omega}^2\Delta_2^2 m_2^2\right), \quad (13)$$

with the result expanded to

$$f_2^*(u_1, m_2) \approx \text{csinc}_{M_1}\left[\frac{M_1}{2}\left(\omega - \frac{2\pi u_1}{M_1}\right)\right]$$

$$\times \exp j\left((\omega - \hat{\omega})\Delta_2 m_2 + a\left(\omega^2 - \hat{\omega}^2\right)\Delta_2^2 m_2^2\right). \quad (14)$$

By limiting

$$a\left(\omega^2 - \hat{\omega}^2\right)^2\Delta_2^2\left(\frac{M_2}{2}\right)^2 \le \frac{\pi}{2} \quad (15)$$

for all ω, a final DFT across m_2 yields approximately

$$f_3(u_1, u_2) \approx \text{csinc}_{M_1}\left[\frac{M_1}{2}\left(\omega - \frac{2\pi u_1}{M_1}\right)\right]$$

$$\times \text{csinc}_{M_2}\left[\frac{M_2\Delta_2}{2}\left((\omega - \hat{\omega}) - \frac{2\pi u_2}{M_2\Delta_2}\right)\right]. \quad (16)$$

The second, and final, best estimate of ω becomes

$$^{(2)}\hat{\omega} \approx \frac{2\pi u_1}{M_1} + \frac{2\pi u_2}{M_2\Delta_2}, \quad (17)$$

with a final resolution of $\rho_2 = (2\pi)/(\Delta_2 M_2)$. A sufficient condition to meet the limit in equation (15) is

$$a\rho_1\Omega\Delta_2^2(M_2/2)^2 \le \pi/2. \quad (18)$$

This, with the migration limit of equation (12), yields the ultimate constraint for a single level of subapertures as

$$\Omega \le \rho_2\, 2^{-1/3}(\pi a)^{-2/3}, \quad (19)$$

where $\rho_2 = 2\pi/(\Delta_2 M_2)$. Equation (19) represents an improvement over equation (5) for $a < 1/(32\pi)$. The benefit of subapertures is thus established.

A similar development for two tiers of subapertures, illustrated in figure 2(c), yields an improved constraint

$$\Omega \le \rho_3\, 2^{-3/4}(\pi a)^{-3/4}. \quad (20)$$

In fact, for N_s tiers of subapertures the ultimate constraint relating resolution and frequency range can be generalized to

$$\Omega \le \rho_{(N_s+1)}\, 2^{\frac{-(2N_s-1)}{(N_s+2)}}(\pi a)^{\frac{-(N_s+1)}{(N_s+2)}} \quad (21)$$

Each additional tier of subapertures improves the constraint, but with diminishing returns. The benefit is derived from the operation in equation (13), namely, the compensation of error terms with a coarse resolution estimate of $\hat{\omega}$. The use of subapertures is constrained by limiting migration to acceptable levels, usually about one current resolution cell over the entire aperture.

4: Polar-format SAR processing limits

Consider a linear-FM chirp radar, collecting echo samples along a flight path at positions indexed by n, $N/2 \le n \le N/2 - 1$, with geometry defined in figure 3. The echoes are deramped and sampled at relative times indexed by i, $I/2 \le i \le I/2 - 1$. The radar operates with

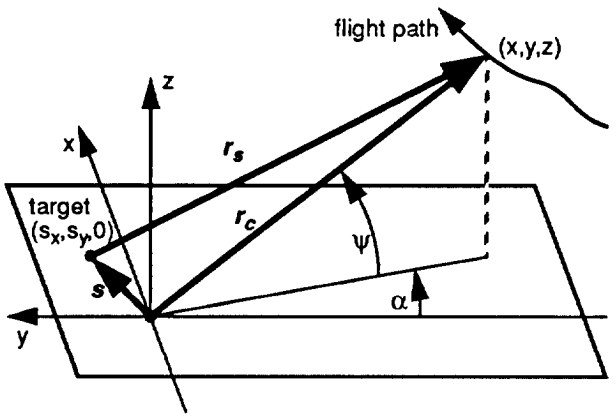

Figure 3. SAR geometry.

center frequency ω_n, chirp rate γ_n, and ADC sample period T_s. With sufficiently long pulses [3], the radar's sampled video signal can be described by

$$X_V(i,n) \approx A(r_s)\ \exp\, j\{\frac{2}{c}[\omega_n + \gamma_n T_s i]\cos\psi_n \cos\alpha_n \times (s_x \tan\alpha_n - s_y + \xi_r(n))\}\ , \quad (22)$$

where $A(r_s)$ represents the amplitude of the echo from the target. The function ξ_r represents spatially variant error terms that can be described with a polynomial in n. By adjusting ω_n and γ_n to compensate for variations in $\cos\psi_n$ and $\cos\alpha_n$, and sampling at equal increments in $\tan\alpha_n$, equation (22) can be simplified to

$$X_V(i,n) \approx A(r_s) \times \exp j\left\{\frac{2\omega_0\cos\psi_0}{c}\left(1+\frac{\gamma_0 T_s}{\omega_0}i\right)(s_x n - s_y + \xi_r(n))\right\}\ , \quad (23)$$

The processing strategy is then to resample along n as a function of $(1+(\gamma_0 T_s i)/\omega_0)$, followed by a 2-dimensional DFT over i and the resampled n. This can be accomplished by employing a chirp-Z transform (CZT) over n that incorporates the resampling, followed by a FFT over i [4]. Recall that the CZT can be implemented with FFTs and vector multiplies. By limiting the largest quadratic term in ξ_r to less than $\pi/2$, then processing in this manner will limit an individual scene to diameter D such that

$$D \le 4\rho_x(\|r_{c0}\|/\lambda_0)^{1/2}, \quad (24)$$

where ρ_x is the nominal resolution in the x-direction at the scene center, $\|r_{c0}\|$ is the nominal range to the scene center, and λ_0 is the nominal wavelength of the radar, $\lambda_0 = 2\pi c/\omega_0$.

5: Polar Formatted Subapertures

Now consider equation (23) where both indices i and n are each divided into a single tier of subapertures, as in figure 2(b), and analogous to equation (6).

$$n = m_1 + \Delta_2 m_2 \quad (25)$$

$$i = k_1 + \mu_2 k_2 \quad (26)$$

Equation (23) then becomes

$$X_V(k_1,k_2,m_1,m_2) \approx A(r_s) \times \exp j\left\{\frac{2\omega_0\cos\psi_0}{c}\left(1+\frac{\gamma_0 T_s \mu_2}{\omega_0}k_2+\frac{\gamma_0 T_s}{\omega_0}k_1\right) \times\left(s_x\Delta_2 m_2 + s_x m_1 - s_y + \xi_r(m_1+\Delta_2 m_2)\right)\right\}. \quad (27)$$

The processing strategy is straightforward and is illustrated in figure 4.

1. perform a CZT across m_1, adjusting output sample spacing as a function of k_1 and k_2. Use the resulting estimate of s_x to compensate the phase of the result.
2. perform a FFT across k_1. Use the result to optimally estimate s_x and s_y to further compensate the phase of the result.
3. perform a CZT across m_2, adjusting output sample spacing as a function of k_2. Use the result to again optimally estimate s_x and s_y to further compensate the phase of the result.
4. perform a FFT across k_2. The result is the complex SAR image.

Note that the error function ξ_r formerly being a polynomial in n, now contains a number of cross product terms between m_1 and m_2. The cross terms that are linear coefficients of the index being transformed manifest

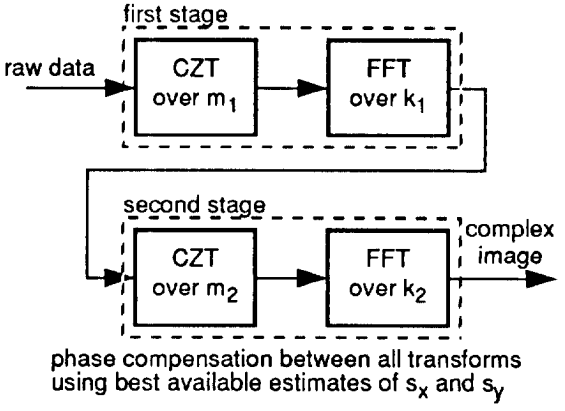

Figure 4. Processing strategy (1 tier)

themselves as migration terms. Migration has the effect of windowing the data and thereby limiting the resolution of succeeding transforms. It is therefor necessary to limit migration to something on the order of one resolution cell across the entire aperture. This is done by limiting subaperture length, and hence subaperture resolution. Since migration affects succeeding transforms, resolution limits due to migration only affect the stages prior to the final transforms, and tend to dominate the effects of other error terms that broaden the impulse response. The final transform pair, however, are over data that contains no cross-product migration terms (or at least none that can't be accommodated by the final CZT) and therefor have resolutions limited by spatially variant phase errors, specifically the quadratic component of the error function.

Migration is limited to about one current (coarse) resolution cell with the following sufficient conditions,

$$D_x^2 \le 8\rho_{x,1}\rho_{x,2}(\|r_{c0}\|/\lambda_0)\,, \tag{28}$$

$$D_y^2 \le 16\rho_{x,1}\rho_{x,2}(\|r_{c0}\|/\lambda_0)\,, \tag{29}$$

and $$\rho_{x,1} \le (4/\lambda_0)\,\rho_{y,1}\rho_{x,2}\cos\psi_0\,. \tag{30}$$

where D_x and D_y are the scene diameters in the x and y directions respectively, $\rho_{x,1}$ and $\rho_{y,1}$ are the resolutions in the x and y directions after the first CZT / FFT transform pair, and $\rho_{x,2}$ and $\rho_{y,2}$ are the resolutions in the x and y directions after the second and final CZT / FFT transform pair. We also define $\delta_{x,1}$ and $\delta_{x,2}$ as the first stage's pixel spacing in the x and y directions respectively.

Limiting the quadratic component of the spatially variant phase errors to about $\pi/2$ limits the final stage CZT / FFT transform pair such that

$$\delta_{x,1} \le (8/D_x)\,\rho_{x,2}^2(\|r_{c0}\|/\lambda_0)\,, \tag{31}$$

and $$\delta_{y,1} \le (16/D_y)\,\rho_{x,2}^2(\|r_{c0}\|/\lambda_0)\,. \tag{32}$$

With the reasonable assumptions that $\rho_{x,2} \ge \lambda_0/2$, $\psi \le \pi/3$, and $\rho_{y,1} = \rho_{x,1} = \delta_{x,1} = \delta_{y,1}$, equations (28) thru (32) will allow an overall limit on scene diameter of

$$D_x, D_y \le 4\rho_{x,2}(\|r_{c0}\|/\lambda_0)^{2/3}\,, \tag{33}$$

which is clearly an improvement over the traditional limit given in equation (24). We also note that if the first stage oversamples its output ($\delta_{x,1} \le \rho_{x,1}$) then the scene diameter limit is further improved by a factor $(\rho_{x,1}/\delta_{x,1})^{1/3}$. This is somewhat similar to the multiple corrections case described in [2].

Note that the initial sampling strategy along with the CZT make each stage a separate polar-format processed image formation step, but allows successive stages to

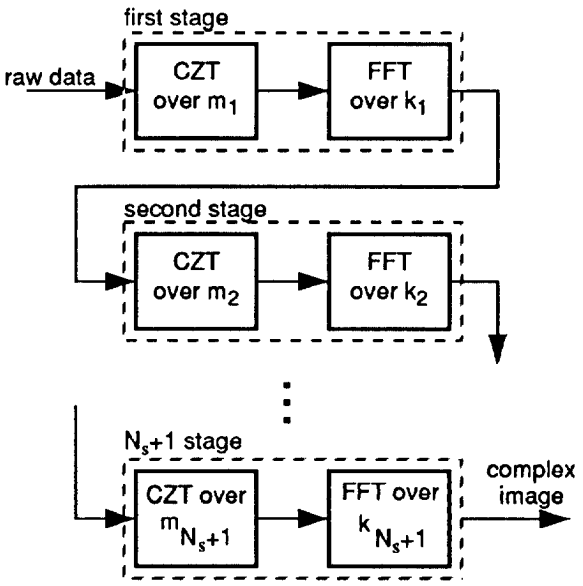

Figure 5. Processing strategy (N_s tiers)

achieve finer resolution. This strategy can be extended in a similar manner to an arbitrary number of tiers of subapertures. Any number N_s tiers will require N_s+1 stages of FFT / CZT pairs, partitioned with indices

$$n = m_1 + \sum_{p=2}^{N_s+1}\left[m_p \prod_{q=2}^{p}\Delta_q\right], \tag{34}$$

and $$i = k_1 + \sum_{p=2}^{N_s+1}\left[k_p \prod_{q=2}^{p}\mu_q\right]. \tag{35}$$

The architecture for such a scheme is illustrated in figure 5. Equation (33) can then be extended to

$$D_x, D_y \le 4\rho_{x,(N_s+1)}(\|r_{c0}\|/\lambda_0)^{\frac{(N_s+1)}{(N_s+2)}}\,. \tag{36}$$

For scene diameters less than this limit, and particularly when image aspect ratios are non-unity, $D_x \ne D_y$, the assumption that each stage's output resolutions be equal in the x and y directions, $\rho_{y,n} = \rho_{x,n}$, may be relaxed, even to the point that a particular transform in some stage collapses to unity length, that is, vanishes. In any case, the relationship between intermediate resolutions need to be chosen to comply with the migration limitations, whereas the relationship between final resolutions need to concern themselves with spatially variant phase error limitations.

One useful derivative processing strategy is to achieve final y-resolution prior to the final CZT and final x-

resolution. This would allow the final CZT to compensate for geometric distortions at the edges of the scene, thereby allowing easier mosaicking of scenes from adjacent apertures into image strips [2].

6: Examples

Consider a SAR operating at 150 MHz, at a nominal elevation angle $\psi_0 = 30^\circ$, and a nominal range $\|r_{c0}\| = 5$ km. Figure 6 illustrates scene diameter limits vs. resolution for processing strategies employing various numbers of tiers of subapertures using equation (36).

The benefit of tiers of subapertures is also illustrated in figure 7, which compares impulse responses of simulated point targets located at various distances from the scene center along the x axis. The data was processed to 1 meter resolution with a -35 dB Taylor window. Other parameters are the same as for figure 6.

7: References

[1] Ausherman, Dale A., Adam Kozma, Jack L. Walker, Harrison M. Jones, Enrico C. Poggio, "Developments in Radar Imaging", IEEE Transactions on Aerospace and Electronic Systems, Vol. AES-20, No. 4, July 1984, pp 363-398.

[2] Burns, B. L., J. T. Cordaro, "SAR image formation algorithm that compensates for the spatially variant effects of antenna motion", SPIE Proceedings Vol 2230, SPIE's International Symposium on Optical Engineering in Aerospace Sensing, Orlando, 4-8 April 1994.

[3] Doerry, A. W., "Patch Diameter Limitations due to High Chirp Rates in Focused Synthetic Aperture Radar Images", IEEE Transactions on Aerospace and Electronic Systems, Vol. AES-30, No. 4, October 1994, pp 1125-1129.

[4] Lawton, Wayne, "A New Polar Fourier Transform for Computer-Aided Tomography and Spotlight Synthetic Aperture Radar", IEEE Transactions on Acoustics, Speech, and Signal Processing, Vol. 36, No. 6, June 1988, pp 931-933.

[5] Perry, R. P., R. C. DiPietro, A. Kozma, J.J. Vaccaro, "SAR Image formation processing using planar subarrays", SPIE Proceedings Vol 2230, SPIE's International Symposium on Optical Engineering in Aerospace Sensing, Orlando, 4-8 April 1994.

[6] Walker, Jack L., "Range-Doppler Imaging of Rotating Objects", IEEE Transactions on Aerospace and Electronic Systems, Vol. AES-16, No. 1, January 1980, pp 23-51.

8: Acknowledgments

This work performed at Sandia National Laboratories is supported by the U.S. Department of Energy under contract DE-AC04-94AL85000.

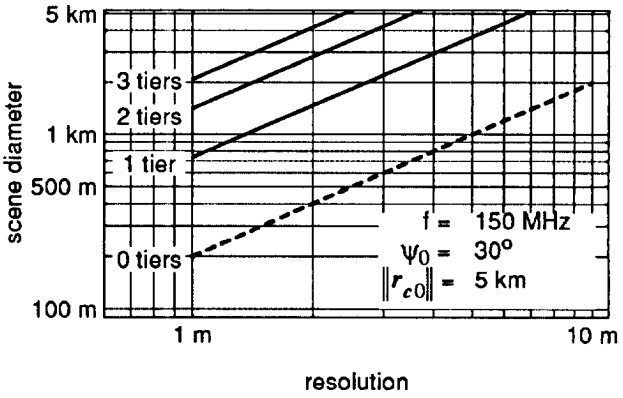

Figure 6. Scene diameter limits vs. resolution

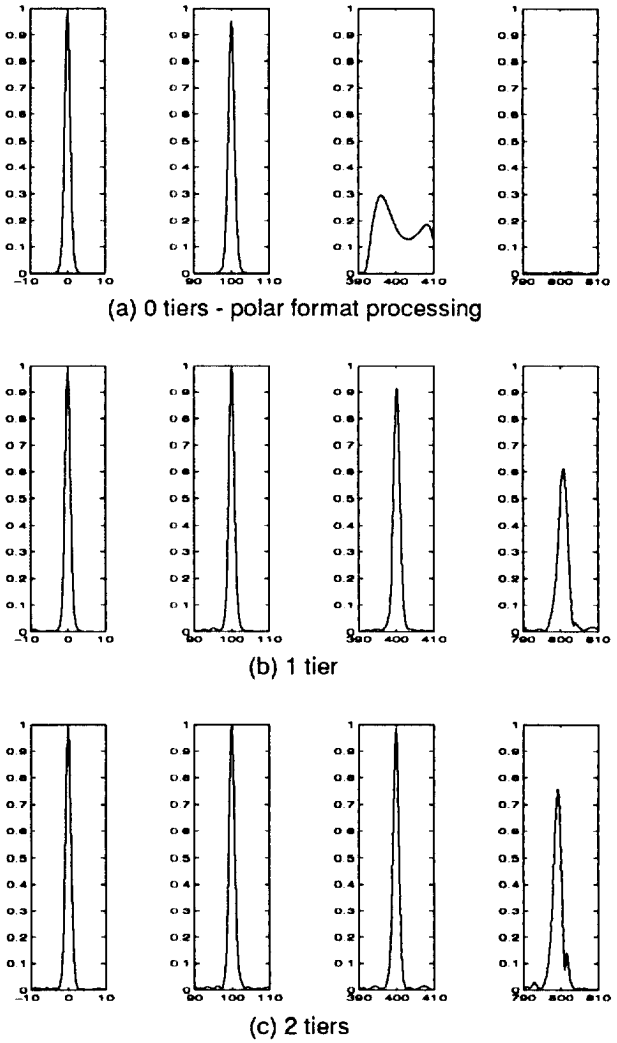

Figure 7. Point target response comparison